11th International Symposium on Turbulence and Shear Flow Phenomena (TSFP11)
Southampton, UK, July 30 to August 2, 2019

LARGE-EDDY SIMULATION OF TURBULENT CHANNEL FLOW AT TRANSCRITICAL STATES

Alexander Doehring
Institute of Aerodynamics and Fluid Mechanics
Department of Mechanical Engineering
Technical University of Munich
Boltzmannstr. 15, 85748 Garching, Germany
alex.doehring@tum.de

Steffen J. Schmidt* and Nikolaus A. Adams†
Institute of Aerodynamics and Fluid Mechanics
Department of Mechanical Engineering
Technical University of Munich
Boltzmannstr. 15, 85748 Garching, Germany

ABSTRACT

We performed a well-resolved large-eddy simulation (LES) of a channel flow solving the fully compressible Navier-Stokes equations in conservative form. An adaptive look-up table method was used for thermodynamic and transport properties. A physically consistent subgrid-scale turbulence model was incorporated, that is based on the Adaptive Local Deconvolution Method (ALDM) for implicit LES. The wall temperatures were set to enclose the pseudo-boiling temperature at a supercritical pressure, leading to strong property variations within the channel geometry. Due to the unilateral heating, asymmetric mean velocity and temperature distributions are observed. Different turbulent Prandtl number formulations are discussed in context of strong property variations.

Introduction

Supercritical fluids, whose pressure and temperature are above its critical values, are used in many engineering applications, as for example in gas turbines, supercritical water-cooled reactors (SCWRs) and liquid rocket engines (LRE). They are characterized by a gas-like diffusivity, a liquid-like density and their surface tension is approaching zero. The latter can be observed in the experimental study with cryogenic jets of Mayer & Tamura (1996). At a supercritical pressure the fluid in the experiments was forming finger-like entities with a continuous phase transition instead of droplets and ligaments. Recent studies, for instance Simeoni *et al.* (2010), disagree with a continuous phase transition, but have shown a supercritical liquid-like (LL) and gas-like (GL) region with a pseudo-boiling line (PBL), which extends the classical liquid-vapor-coexistence line. In this regard, the transcritical condition refers to the temperature variation from compressed fluid ($T < T_{cr}, p > p_{cr}$) to supercritical state ($T > T_{cr}, p > p_{cr}$). Furthermore, strong non-linear property variations are present in the vicinity of the PBL, which are induced by intermolecular repulsive forces. As a consequence, the heat transfer and shear forces in wall bounded flows are affected significantly, leading to poor prediction capabilities of Reynolds-averaged Navier-Stokes simulations (RANS) including established turbulence models (Yoo, 2013). Thus, effects like the heat transfer enhancement as well as the onset of heat transfer deterioration in transcritical and supercritical flows cannot be captured correctly. For this reason, high fidelity data is required to assess the heat transfer prediction capabilities of numerically less expensive turbulence models.

Ma *et al.* (2018) has performed a Direct numerical simulation (DNS) of a transcritical channel flow using an entropy-stable double-flux model in order to avoid spurious pressure oscillations. They have observed the presence of a logarithmic scaling of the structure function and a k^{-1} scaling of the energy spectra, which supports the attached-eddy hypothesis in transcritical flows. A heated transcritical turbulent boundary layer over a flat plate has been investigated by Kawai (2019) with DNS. His study shows large density fluctuations, which exceed Morkovin's hypothesis and lead to a non-negligible turbulent mass flux. In addition, velocity transformations as the van Driest transformation, semi-local scaling by Huang *et al.* (1995) and transformation by Trettel & Larsson (2016) have failed in transcritical boundary layers. This has also been ascertained by Ma *et al.* (2018) and Doehring *et al.* (2018). In this study, we conducted a well-resolved large-eddy simulation (LES) of a transcritical channel flow. We evaluate the turbulent Prandtl number in transcritical flows and assess whether the assumption of a constant value across the boundary layer is justified.

*steffen.schmidt@tum.de
†nikolaus.adams@tum.de

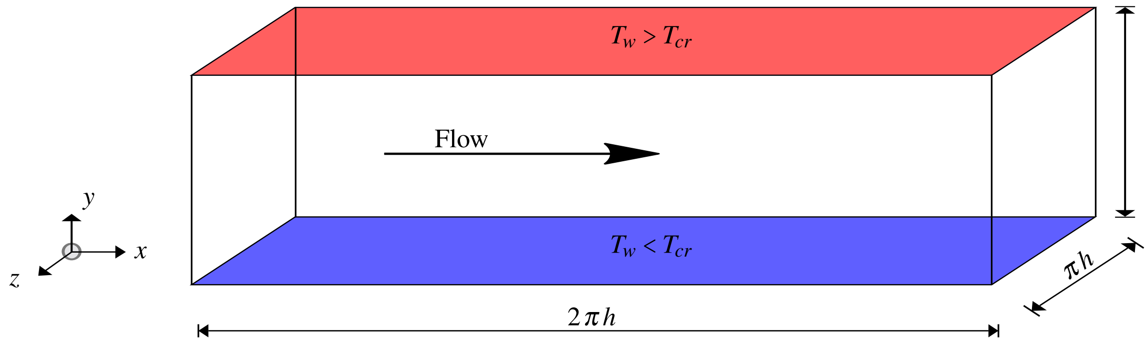

Figure 1. Computational domain with a hot wall above and a cold wall below the critical temperature at supercritical pressure.

Numerical Model

A LES was performed solving the three-dimensional compressible continuity, momentum and total energy equations. The finite-volume method is applied in order to spatially discretize the governing equations on a block structured, curvilinear grid. An explicit second-order low-storage four-stage Runge-Kutta method with enhanced stability region is applied for time advancement (Schmidt *et al.*, 2006). The compact four cell stencil approach by Egerer *et al.* (2016) is used to compute the convective fluxes. A discontinuity detecting sensor functional is used to switch the flux calculation between a linear fourth-order reconstruction for high accuracy and a more stable upwind-biased scheme when high gradients are present. A physically consistent subgrid-scale turbulence model based on the Adaptive Local Deconvolution Method (ALDM) (Hickel *et al.*, 2006, 2014) is implicitly included in the convective flux calculation. Viscous fluxes are determined by a linear second-order centered scheme.

Thermodynamic and transport properties are obtained using an adaptive look-up table method, that is based on the REFPROP database (Lemmon *et al.*, 2013). One table is generated for the fluid domain imposing density and internal energy constraints and a second table is used for the boundary conditions imposing pressure and temperature constraints. Thermodynamic and transport properties are extracted from the tabulated look-up database via trilinear interpolation.

Simulation Setup

A generic channel flow configuration is used to focus this study on transcritical heat transfer and on the impact of non-linear thermodynamic effects on turbulent flows. Periodic boundary conditions are imposed in stream- and spanwise directions, and isothermal no slip boundary conditions are applied at the top and bottom walls. The channel geometry is $2\pi h \times 2h \times \pi h$ in the streamwise, wall-normal and spanwise direction, respectively, see figure 1. The channel half-height h is used as characteristic length. In order to fulfill the resolution requirements at walls, we use a hyperbolic stretching law in wall-normal direction, whereas a uniform grid spacing is used in the stream- and spanwise directions. The grid parameters are summarized in table 1 including the number of grid points in each direction N_x, N_y, N_z and the resolution with respect to wall units $\Delta x^+ = h_x^+ = \Delta x \rho_w u_\tau / \mu_w$, with the friction velocity $u_\tau^2 = (\tau_w / \rho_w)$ and the wall shear stress $\tau_w = (\mu \partial u / \partial y)|_w$. Roughness and gravity effects are not considered in the simulation. The subscript w refers to values at the wall, b to bulk parameters, cr to critical values and pb to values obtained at the pseudo-boiling position.

Table 1. Summary of grid parameters.

$N_x \times N_y \times N_z$	$192 \times 192 \times 192$
$L_x \times L_y \times L_z$	$2\pi h \times 2h \times \pi h$
$h^+_{x_\mathrm{cold}} \times h^+_{x_\mathrm{hot}}$	19.6×9.1
$h^+_{z_\mathrm{cold}} \times h^+_{z_\mathrm{hot}}$	9.8×4.5
$h^+_{y_\mathrm{min,cold}} \times h^+_{y_\mathrm{min,hot}}$	0.66×0.30
$h^+_{y_\mathrm{max,cold}} \times h^+_{y_\mathrm{max,hot}}$	14.2×6.6

Methane is used as working fluid with its critical pressure of $p_{cr} = 4.5992\,\mathrm{MPa}$ and critical temperature of $T_{cr} = 190.564\,\mathrm{K}$. The bulk pressure is $p_b = 4.64\,\mathrm{MPa}$, corresponding to a reduced pressure of $p_r = p_b/p_{cr} = 1.01$. The cold wall temperature is set to $T_{w_c} = 180\,\mathrm{K}$ ($T_{w_c} < T_{cr}$) and the hot wall temperature to $T_{w_h} = 400\,\mathrm{K}$ ($T_{w_h} > T_{cr}$), thus a temperature ratio of $T_{w_h}/T_{w_c} = 2.22$ is obtained. These boundary conditions encompass the pseudo-boiling temperature of $T_{pb} \approx 191\,\mathrm{K}$ at p_b and result in a density ratio of $\rho_{w_c}/\rho_{w_h} = 12.8$. The pseudo-boiling position is determined by means of the specific heat capacity peak at $y \approx -0.98h$.

A body force in the momentum and energy equation is added to maintain a constant mass flux, which corresponds to a bulk velocity of $u_b = 74\,\mathrm{m\,s^{-1}}$. This results in a bulk Reynolds number of $Re_b = (u_b 2h \rho_b)/\mu_b \approx 1.67 \cdot 10^4$. Different friction Reynolds numbers $Re_\tau = (u_\tau \rho_w h)/\mu_w$ are obtained at the walls due to the asymmetrical heating. The value at the cold wall $Re_{\tau_c} = 600$ is approximately 2.2 times larger than at the hot wall with $Re_{\tau_h} = 276$.

Results

In the following, the mean flow properties are analyzed by averaging in time and subsequently in streamwise and spanwise direction after reaching a quasi-stationary state. The Favre average is defined as $\widetilde{\phi} = \overline{\rho \phi}/\overline{\rho}$ and the Reynolds average is an ensemble average denoted with an overline

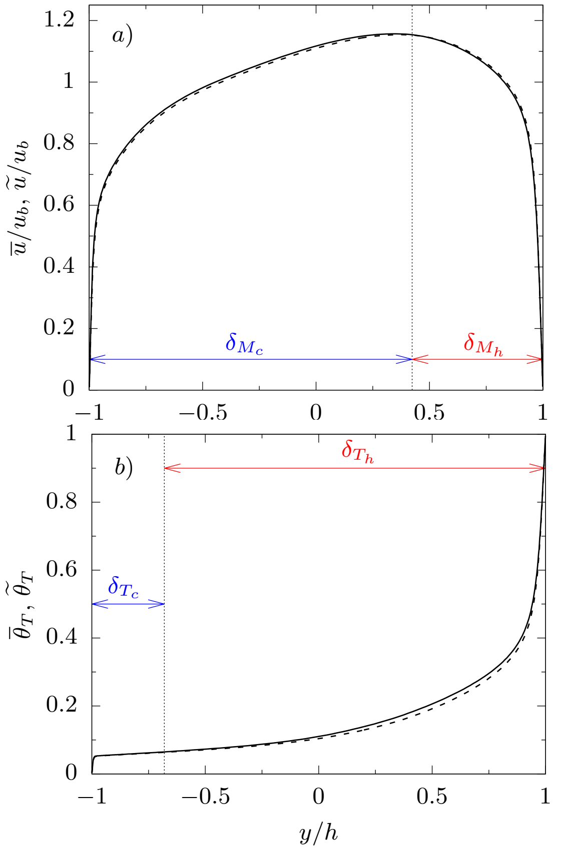

Figure 2. Reynolds (———) and Favre (– – – –) averaged mean velocity (a) and temperature (b) profiles over the channel height. Momentum δ_M and thermal δ_T boundary layer thicknesses are included for the cold and hot side.

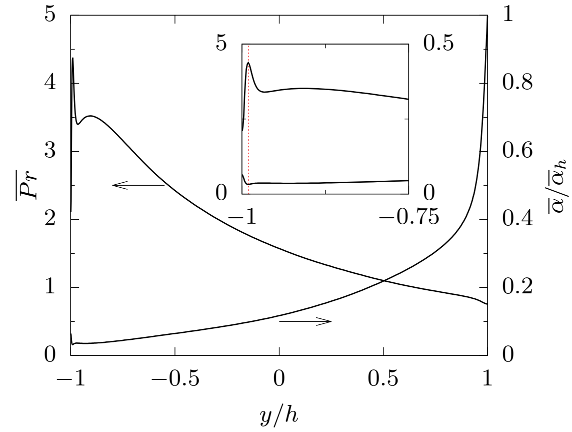

Figure 3. Mean Prandtl number and mean thermal diffusivity profiles over the channel height. The mean thermal diffusivity is scaled with the value at the hot wall $\overline{\alpha}_h$. A zoomed in figure is included for the area close the the cold wall with a red line at the locus of maximum Prandtl number. The axis for mean thermal diffusivity is adjusted.

$\overline{\phi}$. The fluctuations are represented by double prime ϕ'' or single prime ϕ' with respect to Favre and Reynolds average, respectively.

The mean velocity and temperature profiles are shown in figure 2. The temperature is scaled with the wall temperatures $\theta_T = (T - T_{w_c})/(T_{w_h} - T_{w_c})$ and the velocity with the bulk value u_b. Both quantities show a minor difference between the Reynolds and Favre averaging process, which has also been observed by Ma *et al.* (2018). The velocity distribution is shifted towards the hot wall, due to the unilateral heating and the associated thermal expansion. As a consequence, the momentum boundary layer at the cold wall is thicker than at the hot wall $\delta_{M_c} > \delta_{M_h}$. The boundary layer thicknesses are determined by using the locus of zero total shear stress $\tau_{tot} = 0$, indicated by a dotted line. An asymmetry is also present in the temperature profile. The thermal boundary layers are defined as the distance between the wall and the locus of zero heat transfer $\overline{q} = -\overline{\lambda \partial T/\partial y} = 0$ indicated by a dotted line. Thus, the thermal boundary layer thickness at the hot wall is approximately five times the thermal boundary layer thickness at the cold wall.

Due to strong property variations the mean Prandtl number $\overline{Pr} = \overline{\mu c_p/\lambda}$ varies over the channel height from 0.76 to 4.6, see figure 3. Especially close to the pseudo-boiling position at $y_{pb} \approx -0.98h$ strong changes are observed, where momentum diffusivity is dominating and thermal diffusivity $\overline{\alpha} = \overline{\lambda/(\rho c_p)}$ reaches a minimum. This stems from the specific heat capacity peak acting as a heat sink and leading to a flattening of the temperature profile. In addition, a local Prandtl number minimum occurs after the peak value. This local minimum has not been observed in LES with higher bulk pressure (Doehring *et al.*, 2018) or in DNS studies. We attribute this to real gas effects, since the bulk pressure is very close to the critical value of methane.

The highly variable Prandtl number of super- and transcritical channel flows affects the thermal boundary layer and the heat transfer over the walls. Thus, RANS turbulence models, which do not account for a variable Prandtl number, fail in predicting the correct heat transfer (Yoo, 2013). Especially the turbulent Prandtl number Pr_t, which is used as a modeling parameter to close the RANS equation by providing a relationship between the turbulent eddy thermal diffusivity ε_H and turbulent eddy viscosity ε_M, is usually set to a constant value. The strong Reynolds analogy (SRA) assumes, that the turbulent heat transfer and the turbulent momentum transfer are similar resulting in

$$Pr_t = \frac{\varepsilon_M}{\varepsilon_H} = 1. \qquad (1)$$

Experimental and DNS studies have shown, that this simple assumption is not correct, since the turbulent Prandtl number is dependent on the wall distance and the molecular Prandtl number, $Pr_t = f(y^+, Pr)$ (Kays, 1994). It was observed, that Pr_t is relatively constant in the log law region, whereas it is increasing towards the wall and decreasing in the wake region. The following relationship has been determined based on the molecular Prandtl number:

$$Pr_t \leq 1 \quad \text{for} \quad Pr \geq 1 \qquad (2)$$

$$Pr_t > 1 \quad \text{for} \quad Pr \ll 1 \qquad (3)$$

For the analysis of the turbulent Prandtl number in the transcritical LES we included three different formulations:

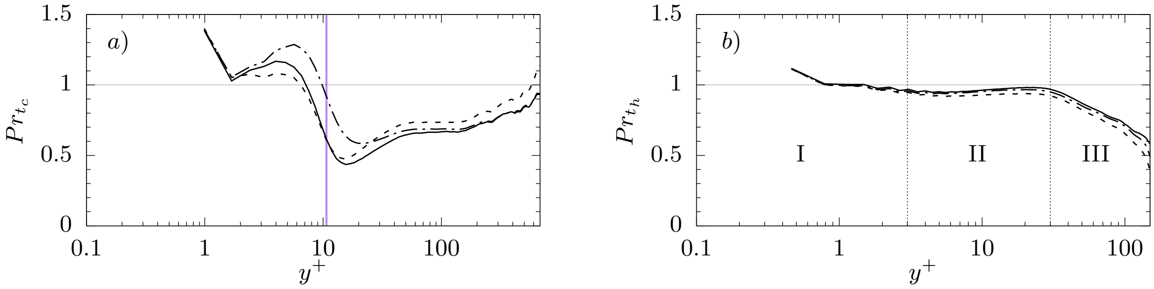

Figure 4. Turbulent Prandtl number at the cold wall (a) and the hot wall (b) over wall units y^+. Included are the incompressible (———), the compressible ($-\cdot-\cdot-$) and the approximated formulation ($----$). The pseudo boiling postion at the cold wall is indicated by a purple line.

Incompressible:

$$Pr_t = \frac{\overline{u'v'}}{\overline{v'T'}} \frac{\partial \overline{T}/\partial y}{\partial \overline{u}/\partial y} \tag{4}$$

Approximation:

$$Pr_t = \frac{\overline{\rho u'v'}}{\overline{\rho v'T'}} \frac{\partial \overline{T}/\partial y}{\partial \overline{u}/\partial y} \tag{5}$$

Compressible:

$$Pr_t = \frac{\widetilde{u''v''}}{\widetilde{v''T''}} \frac{\partial \widetilde{T}/\partial y}{\partial \widetilde{u}/\partial y} \tag{6}$$

Reynolds averaged quantities are used for the incompressible formulation in equation 4, whereas Favre averaged values are included in the compressible definition in equation 6. The approximation is based on the compressible DNS simulation of Huang *et al.* (1995), neglecting the terms $\overline{u''}\,\overline{v''}$ and $\overline{v''}\,\overline{T''}$ in the compressible formulation.

Figure 4 shows the turbulent Prandtl number at the cold and hot wall over the wall normal distance $y^+ = y/l^+$ with $l^+ = \mu_w/(u_\tau \rho_w)$. A relatively constant turbulent Prandtl number is observed at the hot wall, which is similar to ideal gas studies (Kays, 1994). This is not surprising, since the compressibility factor (not shown) is close to one and the molecular Prandtl number does not change too much close to the hot wall ($0.76 < Pr < 1.0$). Towards the hot wall in region I it is increasing up to 1.11, whereas after a local maximum at $y^+ \approx 30$ it is decreasing in region III. Only a small difference between all three formulations is present, leading to the conclusion, that minor compressible effects are present at the hot wall. The turbulent Prandtl number at the cold wall varies strongly close to the pseudo-boiling position indicated by a purple line. All three formulations feature an s-shaped profile at y_{pb} and are increasing in the log-law region. Thus, a constant turbulent Prandtl number is not observed for one of the three formulations.

So far, we used common turbulent Prandtl number formulations from the literature, which are applicable for a wide range of flows, but at a close look all three are not suitable for transcritical channel flows. In general, applying a Favre averaging on the governing equations results in the Reynolds stress tensor $\rho\widetilde{u_i''u_j''}$ for the momentum equations and in the turbulent heat flux $\rho\widetilde{u_i''h''}$ for the energy equation, where h is the enthalpy. Since transcritical and supercritical fluids are characterized by strong non-linear property variations induced by intermolecular repulsive forces in the vicinity of the PBL, the enthalpy is not proportional to the temperature like it is the case for a calorically perfect gas. In figure 5 the NIST data base is used to compare the enthalpy with the relation c_pT, which is used for perfect gas. The profiles are plotted over the scaled temperature range present in the channel at the bulk pressure. At temperatures above $\theta_T > 0.25$ the enthalpy can be approximated using c_pT, since the error $(h - c_pT)/h$ is below 12% (not shown). On the other hand, a strong deviation is observable close to the pseudo-boiling position ($0 < \theta_T < 0.25$), where the enthalpy has a change in the slope, but does not show a peak. For this reason, we suggest to use an enthalpy based turbulent Prandtl number formulation for transcritical channel flows:

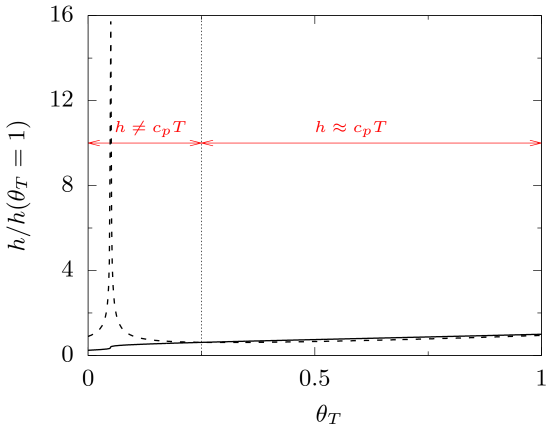

Figure 5. Comparison of enthalpy (———) from the NIST data base with c_pT ($----$) over scaled temperature θ_T at bulk pressure. Enthalpy profiles are normalized with the value at the hot wall.

Enthalpy:

$$Pr_t = \frac{\widetilde{u''v''}}{\widetilde{v''h''}} \frac{\partial \widetilde{h}/\partial y}{\partial \widetilde{u}/\partial y}, \tag{7}$$

Iternal energy:

$$Pr_t = \frac{\widetilde{u''v''}}{\widetilde{v''e''}} \frac{\partial \widetilde{e}/\partial y}{\partial \widetilde{u}/\partial y}. \tag{8}$$

In addition to the enthalpy based formulation, a turbulent Prandtl number based on internal energy is analyzed in order to evaluate the influence of the pressure-density ratio, since $h = e + p/\rho$. Figure 6 shows the turbulent Prandtl number profiles based on the new formulations

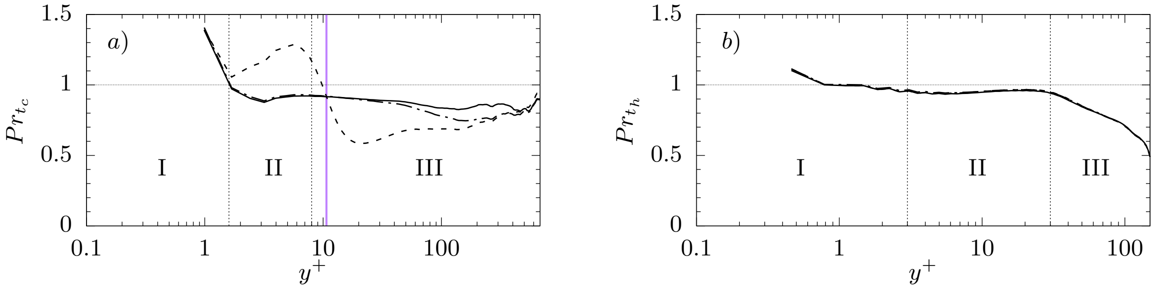

Figure 6. Turbulent Prandtl number at the cold wall (a) and the hot wall (b) over wall units y^+. Included are the compressible (– – – –), the enthalphy based (———) and the internal energy based formulations (–·–·–). The pseudo boiling postion at the cold wall is indicated by a purple line.

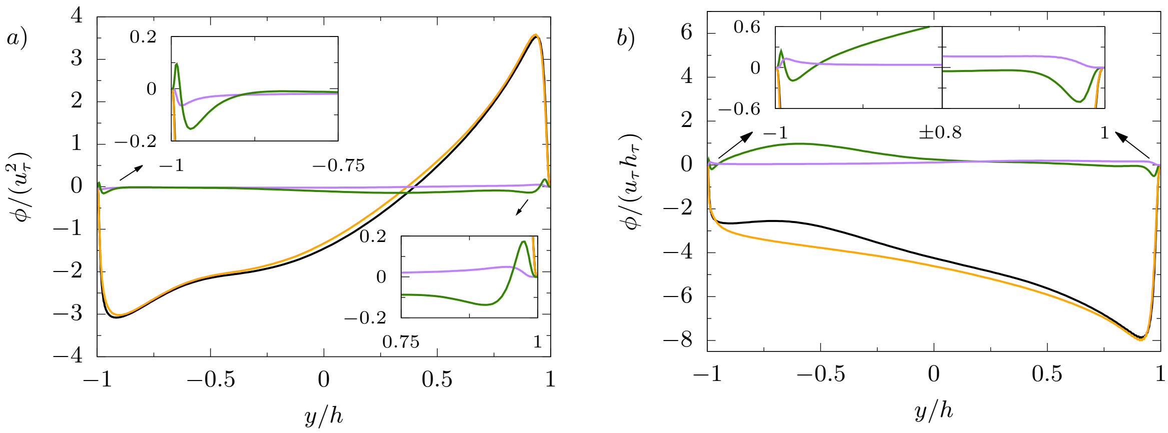

Figure 7. Terms of Favre averaged turbulent shear stress (a) and turbulent heat flux (b) over wall normal distance. ϕ represents $\widetilde{u''v''}$ and $\widetilde{v''h''}$ (———); $\overline{u'v'}$ and $\overline{v'h'}$ (———); $\overline{u''}\,\overline{v''}$ and $\overline{v''}\,\overline{h''}$ (———); $\overline{\rho' u' v'}/\overline{\rho}$ and $\overline{\rho' v' h'}/\overline{\rho}$ (———). Subfigures are included to enlarge the profiles close to the walls.

at the cold and hot wall. For comparison, also the compressible formulation using temperature is included. Since the specific heat capacity change is relatively small in the hot wall boundary layer, the enthalpy can be approximated using the relation for a calorically perfect gas $h \approx c_p T$. For this reason, all three profiles coincide and feature a relatively constant value in region II at the hot wall. In figure 6a), in contrast to the compressible formulation with an s-shaped profile, the enthalpy based one has a relatively constant distribution over the boundary layer. Furthermore, region I and II are showing a distribution similar as for the hot wall. An considerable deviation between the enthalpy and internal energy based formulations is found in region III, where the latter is decreasing faster, thus, the pressure-density ratio is neglectable in the viscous sublayer.

Based on the work of Huang *et al.* (1995), we analyze the terms of the Favre averaged turbulent shear stress and turbulent heat flux:

$$\widetilde{u''v''} = \overline{u'v'} - \overline{u''}\,\overline{v''} + \frac{\overline{\rho' u' v'}}{\overline{\rho}}, \tag{9}$$

$$\widetilde{v''h''} = \overline{v'h'} - \overline{v''}\,\overline{h''} + \frac{\overline{\rho' v' h'}}{\overline{\rho}}. \tag{10}$$

His analysis has shown, that the second term in equation 9 is at least one order of magnitude smaller than the other two in compressible channel flows, thus, it can be neglected. For the normalization of the terms the friction velocity and enthalpy $h_\tau = B_q h_w$ with the heat flux parameter $B_q = q_w/(\rho_w h_w u_\tau)$ are used. Figure 7a) shows, that the second and third term of turbulent shear stress are an order of magnitude smaller than the first term. The second term is confined to the viscous sublayer and reaches 10% and 5% of the total diffusivity at the hot and cold wall, respectively. The triple correlation is only relevant at the cold wall reaching up to 30%, whereas it can be neglected at the hot wall. The second term in figure 7b) is small enough at both walls in order to be neglected. The third term of the turbulent heat flux is affected by the pseudo-boiling changing the sign, which is not present at the hot wall. Additionally, the term has a significant bump at the cold wall within the logarithmic layer. This bump affects the total heat transfer profile and is responsible for the decrease of the turbulent Prandtl number in region III.

The turbulent Prandtl number is also used in context of Reynolds analogies in order to deduce a relationship between temperature and velocity. Zhang *et al.* (2014) derived a generalized Reynolds analogy (GRA) for flows over diabatic walls by introducing a local recovery factor for the effect of $Pr \neq 1$. The resulting temperature-velocity relationship assumes a constant recovery factor based on the molecular Prandtl number at the wall rather than varying values within the boundary layer, see equation 11. In addition, a calorically perfect gas with $h = c_p T$ and a constant specific heat capacity have been implied.

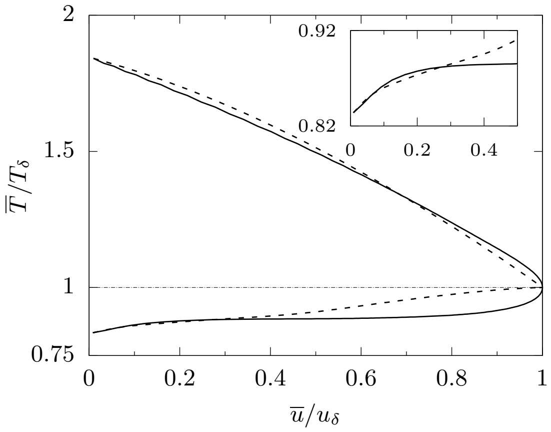

Figure 8. Mean temperature profile (———) over mean velocity scaled with values obtained at the momentum boundary layer edge indicated with the subscript δ. GRA by Zhang *et al.* (2014) is represented by (– – – –).

$$\frac{\overline{T}}{\overline{T}_\delta} = \frac{\overline{T}_w}{\overline{T}_\delta} + \frac{\overline{T}_{rg} - \overline{T}_w}{\overline{T}_\delta}\frac{\overline{u}}{\overline{u}_\delta} + \frac{\overline{T}_\delta - \overline{T}_{rg}}{\overline{T}_\delta}\left(\frac{\overline{u}}{\overline{u}_\delta}\right)^2. \qquad (11)$$

The relationship includes the recovery temperature $\overline{T}_{rg}$ and the recovery factor r_g. The subscript δ refers to values at the momentum boundary layer edge. Due to strong property variations, we replaced the constant specific heat and the molecular Prandtl number at the wall with the distribution over the wall normal distance. In figure 8 the mean temperature is plotted over the mean velocity including equation 11. The GRA works well at the hot wall, where only mild molecular Prandtl number and heat capacity changes are present. At the cold wall the GRA fails, which can be ascribed to the assumptions made in the derivation.

Conclusion

We investigated a turbulent transcritical channel flow imposing different wall temperatures, thus, enclosing the pseudo-boiling temperature using a well-resolved LES. The fully compressible Navier-Stokes equations have been solved and an adaptive look-up table method has been used for thermodynamic and transport properties. The mean velocity distribution is shifted towards the hot wall leading to different boundary layer thicknesses. Strong property variations in the vicinity of the pseudo-boiling position are observed by means of the molecular Prandtl number, which showed a peak value close to the cold wall. The peak correlates with minimum heat diffusivity leading to a flattening of the mean temperature. The turbulent Prandtl number is relatively constant and not dependent on the turbulent eddy thermal diffusivity definition at the hot wall, which was ascribed to mild changes of thermodynamic properties. Only the enthalpy based turbulent Prandtl number was unaffected by the pseudo-boiling at the cold wall, whereas the temperature based ones show strong variations. The GRA by Zhang *et al.* (2014) showed a good agreement at the hot wall, but failed in regions with strong property variations.

Acknowledgments

The authors gratefully acknowledge the financial support provided by the German Research Foundation (Deutsche Forschungsgemeinschaft-DFG) within the framework of the Sonderforschungsbereich Transregio 40, SFB-TRR40 (Technological foundations for the design of thermally and mechanically highly loaded components of future space transportation systems). Computational resources have been provided by the Leibniz Supercomputing Centre Munich (LRZ).

REFERENCES

Doehring, A., Schmidt, S. J. & Adams, N. A. 2018 Numerical Investigation of Transcritical Turbulent Channel Flow. In *2018 Joint Propulsion Conference*.

Egerer, C. P., Schmidt, S. J., Hickel, S. & Adams, N. A. 2016 Efficient implicit LES method for the simulation of turbulent cavitating flows. *Journal of Computational Physics* **316**, 453–469.

Hickel, S., Adams, N. A. & Domaradzki, J. A. 2006 An adaptive local deconvolution method for implicit LES. *Journal of Computational Physics* **213**, 413–436.

Hickel, S., Egerer, C. P. & Larsson, J. 2014 Subgrid-scale modeling for implicit large eddy simulation of compressible flows and shock-turbulence interaction. *Physics of Fluids* **26**.

Huang, P. G., Coleman, G. N. & Bradshaw, P. 1995 Compressible turbulent channel flows: DNS results and modelling. *Journal of Fluid Mechanics* pp. 185–218.

Kawai, S. 2019 Heated transcritical and unheated non-transcritical turbulent boundary layers at supercritical pressures. *Journal of Fluid Mechanics* **865**, 563–601.

Kays, W. M. 1994 Turbulent Prandtl Number—Where Are We? *Journal of Heat Transfer* **116**, 284–295.

Lemmon, E. W., Huber, M. L. & McLinden, M. O. 2013 NIST Standard Reference Database 23: Reference Fluid Thermodynamic and Transport Properties-REFPROP, Version 9.1. *National Institute of Standards and Technology* .

Ma, P. C., Yang, X. I. A. & Ihme, M. 2018 Structure of wall-bounded flows at transcritical conditions. *Physical Review Fluids* **3** (3), 1–24.

Mayer, W. & Tamura, H. 1996 Propellant injection in a liquid oxygen/gaseous hydrogen rocket engine. *Journal of Propulsion and Power* **12** (6), 1137–1147.

Schmidt, S. J., Sezal, I. H. & Schnerr, G. H 2006 Compressible simulation of high-speed hydrodynamics with phase change. In *European Conference on Computational Fluid Dynamics*.

Simeoni, G. G., Bryk, T., Gorelli, F. A., Krisch, M., Ruocco, G., M., Santoro & T., Scopigno 2010 The Widom line as the crossover between liquid-like and gas-like behaviour in supercritical fluids. *Nature Physics* **6**, 503 – 507.

Trettel, A. & Larsson, J. 2016 Mean velocity scaling for compressible wall turbulence with heat transfer. *Physics of Fluids* **28** (2), 026102.

Yoo, J. Y. 2013 The Turbulent Flows of Supercritical Fluids with Heat Transfer. *Annual Review of Fluid Mechanics* **45** (1), 495–525.

Zhang, Y.-S., Bi, W.-T., Hussain, F. & She, Z.-S. 2014 A generalized Reynolds analogy for compressible wall-bounded turbulent flows. *Journal of Fluid Mechanics* **739**, 392–420.